Chinese Chemical Letters 37 (2026) 112136

Contents lists available at ScienceDirect

Chinese Chemical Letters

journal homepage: www.elsevier.com/locate/cclet

Enhanced efficiency of solution-processed lanthanide-based OLEDs *via* ligand engineering: Tuning excited-state lifetime and charge transport with Se-modified ligand

Zhipeng Guo[a,b], Arseny Gladkikh[a], Egor Latipov[c], Andrey Vashchenko[d], Yaxuan Liu[e], Alexey Medvedko[f], Alexander Goloveshkin[g], Olga Maloshitskaya[h], Alexey Alexandrov[i], Aowei Zhou[a,b], Yiming Yin[a,b], Yanan Zhu[b,*], Hong Meng[b,j,*], Valentina Utochnikova[a,*]

[a] *Faculty of Materials Science, M. V. Lomonosov Moscow State University, Moscow 119991, Russia*
[b] *Faculty of Materials Science, Shenzhen MSU-BIT University, Shenzhen 518172, China*
[c] *Institute of Nanotechnology of Microelectronics of the Russian Academy of Sciences (INME RAS), Moscow 115487, Russia*
[d] *P. N. Lebedev Physical Institute, Moscow 119992, Russia*
[e] *Beijing Institute of Technology, Beijing 100081, China*
[f] *N.D. Zelinsky Institute of Organic Chemistry RAS, Moscow 119991, Russia*
[g] *A. N. Nesmeyanov Institute of Organoelement Compounds, Moscow 119334, Russia*
[h] *Department of Chemistry, Lomonosov Moscow State University, Moscow 119991, Russia*
[i] *A. N. Frumkin Institute of Physical Chemistry and Electrochemistry RAS, Moscow 119071, Russia*
[j] *School of Advanced Materials, Peking University Shenzhen Graduate School, Shenzhen 518055, China*

ARTICLE INFO

Article history:
Received 25 September 2025
Revised 17 November 2025
Accepted 18 November 2025
Available online 19 November 2025

Keywords:
Organic light-emitting diode
Lanthanide complexes
High efficiency
Solution-processed OLED
Se-modified ligand

ABSTRACT

Lanthanide complexes attract significant attention for their narrow-band emission with nearly constant wavelengths; however, developing high-efficiency lanthanide-complex organic light-emitting diode (OLED) devices and methodologies remains a primary research focus. We selected neutral ligands [1,2,5]thiadiazolo[3,4-*f*][1,10]phenanthroline (TDZP) and its selenium (Se)-containing counterpart, [1,2,5]selenadiazolo[3,4-*f*][1,10]phenanthroline (SDZP), to form complexes with dibenzoylmethane (Hdbm). Detailed investigations combining theoretical calculations and experimental data reveal synergistic effects between excited-state lifetimes and charge carrier mobility in enhancing quantum efficiency. All the devices demonstrated characteristic lanthanide ion emission, with the $Eu(dbm)_3SDZP$-based OLED achieving remarkable electroluminescent performance: a maximum quantum efficiency (EQE_{max}) of 6.7 %, ranking among the highest reported values for Eu-based complex OLEDs. This integrated computational-experimental approach establishes a viable strategy for developing high-efficiency lanthanide-complex OLEDs.

© 2026 Published by Elsevier B.V. on behalf of Chinese Chemical Society and Institute of Materia Medica, Chinese Academy of Medical Sciences.

The organic light-emitting diodes (OLEDs) have fundamentally revolutionized both display technologies and solid-state lighting solutions, primarily due to their exceptional color purity, remarkably wide viewing angles, and inherent compatibility with flexible plastic substrates [1]. While significant progress has undeniably been made in developing highly efficient fluorescence and phosphorescent emitters based on transition metals such as zinc, palladium, and other elements, a growing scientific interest has recently emerged in utilizing lanthanide complexes [2–6]. This interest arises from their unique narrow-line, essentially monochromatic emission characteristics and exceptionally high color purity, which are derived from well-shielded f-f electronic transitions. This property allows OLEDs to meet stringent color standards (*e.g.*, Rec. 2020 for ultra-high-definition displays) without the need for additional color filters, thereby reducing light loss and enhancing energy efficiency [7,8].

In the context of biomedicine, red and near-infrared (NIR)-emitting OLEDs have garnered significant interest due to the deeper tissue penetration capability of red/NIR wavelengths, which experience reduced scattering and absorption in biological media. While extreme brightness is often unnecessary for such devices given their typical deployment in direct contact with target regions, high luminous efficiency remains critically important as

* Corresponding authors.
E-mail addresses: zhuyn@smbu.edu.cn (Y. Zhu), menghong@pku.edu.cn (H. Meng), valentina.utochnikova@gmail.com (V. Utochnikova).

https://doi.org/10.1016/j.cclet.2025.112136
1001-8417/© 2026 Published by Elsevier B.V. on behalf of Chinese Chemical Society and Institute of Materia Medica, Chinese Academy of Medical Sciences.

it translates to lower operational power consumption, a critical advantage for battery-dependent wearable or implantable medical apparatus, while concurrently mitigating undesired heat generation during interface with delicate biological tissues [9–11]. To address these efficiency requirements, Eu^{3+} and Yb^{3+} complexes emerge as particularly promising lanthanide candidates; Eu^{3+} exhibits characteristically intense red emission from its hypersensitive $^5D_0 \rightarrow {}^7F_2$ transition, whereas Yb^{3+} delivers efficient near-infrared luminescence *via* $^2F_{5/2} \rightarrow {}^2F_{7/2}$ transition. These properties prove highly valuable for advanced optoelectronic applications, particularly in human bio-signal detection [8], with complementary research from our team demonstrating the practical feasibility of utilizing both complexes as key components in next-generation pulse oximeters [12].

Despite these advantages, the intrinsic luminescent properties of Eu^{3+} and Yb^{3+} complexes present a critical barrier to achieving the required luminous efficiency outlined above. Their characteristically long excited-state lifetimes (τ) directly limit achievable brightness and operational efficiency in OLED architectures [13]. Critically, this extended lifetime significantly increases the probability of detrimental processes like triplet-triplet annihilation (TTA), where accumulated long-lived excitons collide and decay non-radiatively. The efficiency of this loss pathway is further exacerbated by imbalanced electron and hole transport within the emitting layer (EML), as poor or mismatched charge mobility (μ) leads to localized charge accumulation and consequently, higher local triplet exciton densities. Consequently, advancing such systems necessitates strategic development of novel ligand architectures coupled with rigorous optimization of charge mobility, encompassing both electron and hole transport, within EML. This dual focus is imperative because the ultimate device performance depends critically on two interlinked factors: The ligand sensitization efficacy toward lanthanide ions and the EML charge-transport properties.

In this study, to develop Eu- and Yb-based OLED devices with enhanced luminescence properties, we selected neutral ligands [1,2,5]thiadiazolo[3,4-*f*][1,10]phenanthroline (TDZP), containing sulfur (S), and its structurally analogous but heavier selenium (Se)-containing counterpart, [1,2,5]selenadiazolo[3,4-*f*][1,10]phenanthroline (SDZP). Dibenzoylmethane (Hdbm) was chosen as the anionic ligand. This selection was driven by TDZP record-high brightness and efficiency achieved in previous lanthanide-complex OLEDs [14,15], and dbm^- proven ability to deliver the highest brightness when used in Eu-based complexes as the OLED emitting layer [16,17]. Thus, the objects of this study were mixed-ligand complexes $Ln(dbm)_3L$ (Fig. 1a), in which $Eu(dbm)_3$TDZP has also been reported by our group in previous work [18].

The complexes $Ln(dbm)_3L$ (Ln = Yb^{3+} or Eu^{3+}, L = TDZP or SDZP) were synthesized *via* an exchange reaction in ethanol solution using $YbCl_3{\cdot}6H_2O$ or $EuCl_3{\cdot}6H_2O$, Hdbm, the respective neutral ligand (TDZP or SDZP), and NEt_3. The method of synthesis is described in references [19] and [20]. Single crystals of $Eu(dbm)_3$TDZP and $Eu(dbm)_3$SDZP were successfully grown by slow evaporation of their acetonitrile solutions. Both complexes are monomeric. In each, the central Eu^{3+} ion is coordinated by three dbm^- anions and one TDZP or SDZP molecule, resulting in a coordination number (CN) of 8 and a twisted square antiprismatic (TSAP) geometry (Figs. 1b and c).

Powder X-ray diffraction (PXRD) data (Fig. S1 in Supporting information) revealed that among the four synthesized complexes, $Yb(dbm)_3$SDZP was amorphous, while the other three are crystalline. The composition of all compounds was confirmed by matrix-assisted laser desorption/ionization mass spectrometry (MALDI MS) data (Figs. 1d and e), scanning electron microscopy (SEM) and X-ray spectroscopy data (Fig. 1f and Table S1 in Supporting information), thermogravimetric analysis (TGA) data (Fig. S2 in Supporting information), Fourier transform infrared (FTIR) spectroscopy data (Fig. S3 in Supporting information), and ^{1}H NMR spectroscopy data (Fig. S4 in Supporting information).

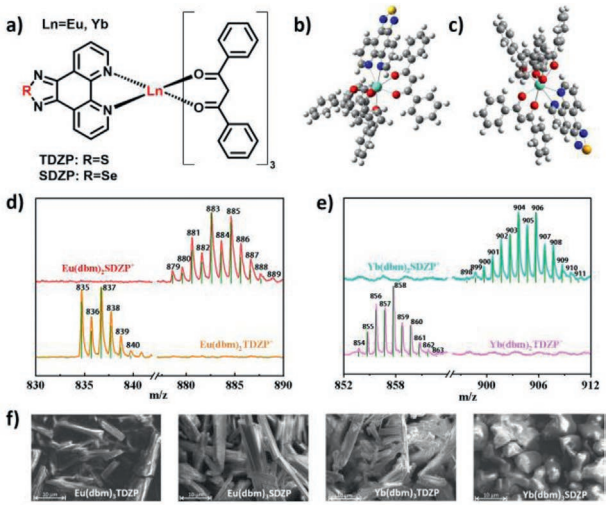


Fig. 1. (a) Structural formula of mixed-ligand complex $Ln(dbm)_3L$. (b, c) Crystal structures of complexes: $Eu(dbm)_3$TDZP and $Eu(dbm)_3$SDZP. (d, e) MALDI MS spectrum of $Ln(dbm)_2L^+$ with the theoretical isotopic distribution of these complexes indicated by green sticks (calculated using https://www.chemcalc.org/). (f) SEM image of $Ln(dbm)_3L$.

MALDI MS spectra (Figs. 1d and e) exhibited strong signals corresponding to the fragment ions $Eu(dbm)_2L^+$ and $Yb(dbm)_2L^+$, formed by the loss of one dbm^- anion from the parent complexes. This behavior was earlier observed for similar mixed-ligand diketonates [21].

The SEM images (Fig. 1f) revealed that the $Eu(dbm)_3$TDZP complex forms well-defined rod-like crystals, indicating oriented crystal growth influenced by the TDZP ligand, whereas $Eu(dbm)_3$SDZP exhibits irregular crystalline aggregates with a rough morphology, attributable to specific steric and electronic effects of the SDZP ligand. The $Yb(dbm)_3$TDZP complex maintains a similar rod-like structure to its Eu counterpart but features smaller crystal dimensions and higher packing density, consistent with Yb^{3+} smaller ionic radius compared to Eu^{3+}; conversely, $Yb(dbm)_3$SDZP displays a completely amorphous morphology characterized by equiaxed grains.

To determine frontier molecular orbital (FMO) distributions and electron and hole mobilities, density functional theory (DFT) and time-dependent density functional theory (TD-DFT) calculations were performed for the four complexes using the Gaussian09, Multiwfn and AMS programs [22]. Calculations for ligands Hdbm, TDZP, and SDZP in the ground state employed the B3LYP/6–31G(d,p) level, with relevant results presented in Fig. S5 and Table S2 (Supporting information). For the complexes, the central metal atom and ligand geometries in the ground state were optimized using the PBE0/SDD and PBE0/6–31G(d,p) level, respectively; these optimized structures were subsequently subjected to wavefunction stability tests using PBE0/SDD and PBE0/6–311G(d,p), all incorporating Grimme's D3 dispersion correction with the Becke Johnson (BJ) damping scheme [23–25], with relevant results presented in Fig. 2 [26,27]. All calculations successfully converged.

According to Fig. 2, the highest occupied molecular orbital (HOMO) of the complexes is primarily localized on the carbonyl groups and phenyl rings of the anionic dbm^- ligand, while the lowest unoccupied molecular orbital (LUMO) distribution is more diffuse, and its energy level is closely related to the ligand. In the Eu-based complexes, the α-LUMO is distributed around the central metal ion and the β-LUMO resides on the neutral TDZP or

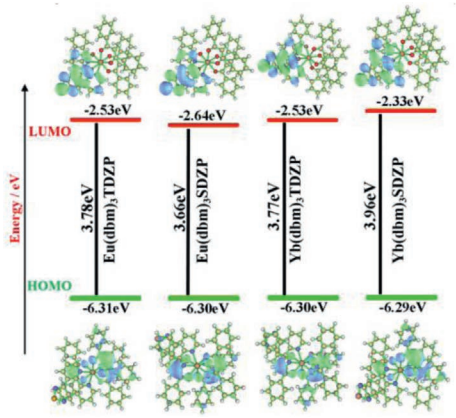


Fig. 2. The calculated HOMO and LUMO distributions of complexes.

SDZP ligand; conversely, the Yb-based complexes exhibit the opposite pattern (Figs. S6 and S7 in Supporting information).

To gain deeper insight into the electron and hole transport properties of complexes with different ligands, we calculated the charge carrier mobility based on single-crystal structures of two europium-based complexes (Fig. S8 in Supporting information), with results presented in Figs. 3a, b and Tables S3 and S4 (Supporting information) [28–32]. The $Eu(dbm)_3TDZP$ complex exhibits higher hole and electron transfer integral values, particularly in the P-dimer configuration. In contrast, $Eu(dbm)_3SDZP$ displays significantly lower transfer integrals, notably with values in the parallel packing (P-dimer) configuration lower than those of $Eu(dbm)_3TDZP$; under transverse packing direction (T_1-T_5), transfer integrals for both complexes approach zero. However, $Eu(dbm)_3TDZP$ exhibits higher λ for both transport modes, indicating significant kinetic barriers and lower transport efficiency. Conversely, $Eu(dbm)_3SDZP$ shows markedly lower λ for both modes, suggesting superior transport capability and favorable conditions for charge carrier migration. Experimentally measured mobility further confirms this observation: complexes with SDZP as the neutral ligand exhibit higher mobility than those with TDZP (Fig. 3c and Fig. S9 in Supporting information).

To study the photoluminescent properties (Table S6 in Supporting information) of the complexes under different states, we measured their excitation spectra, photoluminescence (PL) spectra, PL quantum yields (PLQY), and excited-state lifetimes (Fig. 4 and Figs. S10–S12 in Supporting information) both in the powder state and as spin-coated thin films from tetrahydrofuran (THF) solutions (5 g/L).

For Eu-complexes in powder form, excitation peaks appear at ~420 nm (Fig. 4a), whereas in THF this peak shifts to ~350 nm (Fig. 4b). The emission spectra of Eu^{3+} complexes in powder (Fig. 4c) and THF films (Fig. 4d) exhibit characteristic transitions:

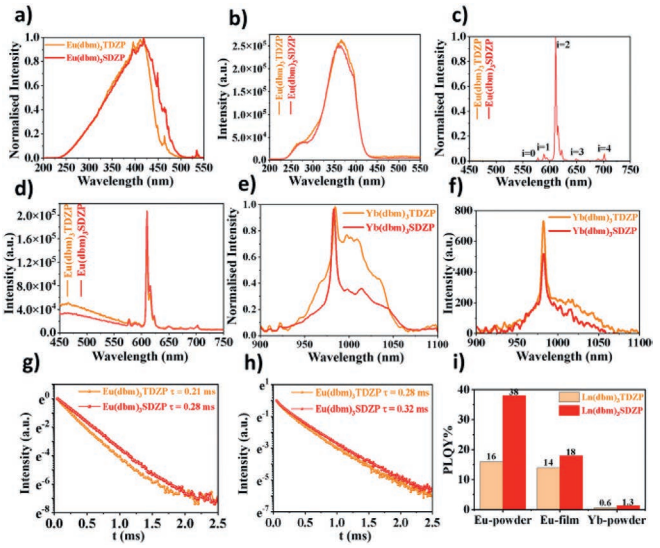


Fig. 4. Absorption spectra of (a) powder and (b) film of $Eu(dbm)_3TDZP$ and $Eu(dbm)_3SDZP$ complexes. Luminescence spectra of (c) powder (λ_{ex} = 420 nm, 298 K) and (d) film (λ_{ex} = 360 nm, 298 K) of $Eu(dbm)_3TDZP$ and $Eu(dbm)_3SDZP$ complexes. Luminescence spectra of (e) powder and (f) film of $Yb(dbm)_3TDZP$ and $Yb(dbm)_3SDZP$ complexes. Luminescence decay curves of (g) powder and (h) film of $Eu(dbm)_3TDZP$ and $Eu(dbm)_3SDZP$ complexes. (i) PLQY (%) of four pure complexes in different form. Films were deposited from a 5 g/L solution of the pure complex (without doping) in THF, then heated at 120 °C for 20 min.

578 nm ($^5D_0 \rightarrow {}^7F_0$), 590 nm ($^5D_0 \rightarrow {}^7F_1$, magnetic dipole radiation), 611 nm ($^5D_0 \rightarrow {}^7F_2$, electric dipole radiation, hypersensitive transition), along with peaks at 650 nm ($^5D_0 \rightarrow {}^7F_3$) and 702 nm ($^5D_0 \rightarrow {}^7F_4$). The significantly higher intensity of the $^5D_0 \rightarrow {}^7F_2$ peak relative to $^5D_0 \rightarrow {}^7F_1$ indicates high monochromaticity; the narrow linewidth of the unsplit, symmetric $^5D_0 \rightarrow {}^7F_0$ peak confirms high compound purity and uniform metal-ion coordination environments. Emission spectra of both Yb-containing complexes (Figs. 4e and f) display characteristic Yb^{3+} features: a characteristic emission peak at ~984 nm in the NIR region corresponding to the $^2F_{5/2} \rightarrow {}^2F_{7/2}$ transition, typical for Yb^{3+} ions in octahedral coordination.

Both the luminescence lifetimes and PLQYs are higher for complexes incorporating the SDZP ligand compared to those with TDZP, for both Eu^{3+} and Yb^{3+} (Figs. 4g–i). This difference can be attributed to the enhanced heavy-atom effect in SDZP, which promotes spin-orbit coupling, facilitating more efficient intersystem crossing and energy transfer from the ligand to the lanthanide center. As a result, nonradiative decay pathways are suppressed, leading to longer emission lifetimes and higher quantum yields. The extended lifetimes are particularly indicative of a reduction in nonradiative deactivation processes, such as vibrational quench-

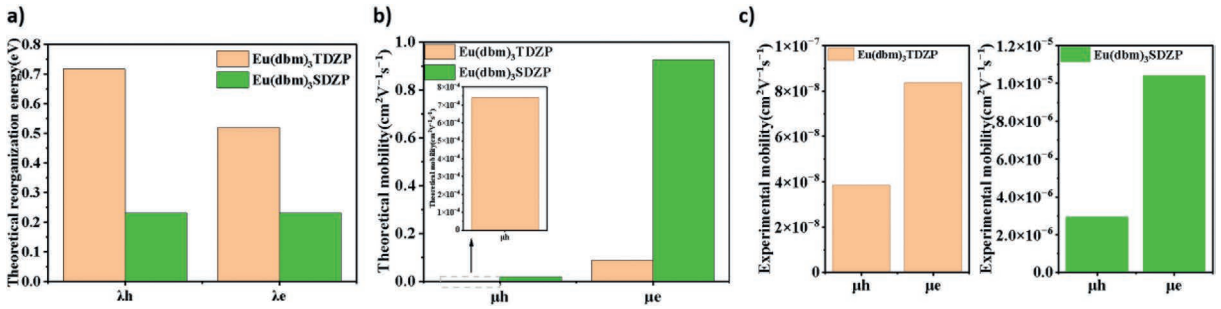


Fig. 3. (a) Reorganisation energies (λ) of $Eu(dbm)_3TDZP$ and $Eu(dbm)_3SDZP$ complexes in different charge states. (b) Theoretical and (c) experimental carrier mobility (μ) of $Eu(dbm)_3TDZP$ and $Eu(dbm)_3SDZP$.

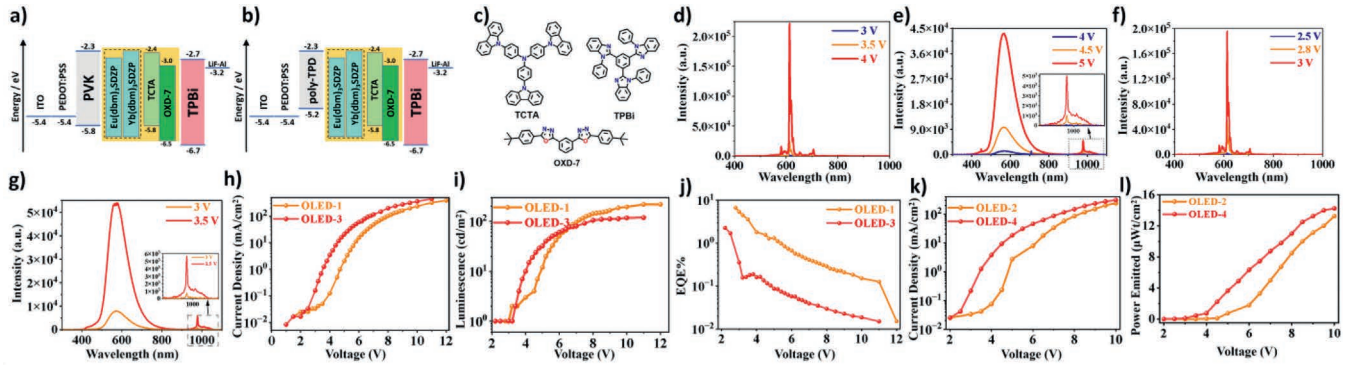


Fig. 5. (a) The schematic energy level diagram of related materials used in the fabrication of the OLED devices 1–2. (b) The schematic energy level diagram of related materials used in the fabrication of the OLED 3–4. (c) Chemical structures of functional layers of the devices based on $Ln(dbm)_3SDZP$. EL spectra of (d) OLED-1, (e) OLED-2, (f) OLED-3, (g) OLED-4. Characteristics of OLED-1 and OLED-3: (h) current density–voltage (*J–V*), (i) luminance–voltage (*L–V*), (j) external quantum efficiency with the voltage. Characteristics of OLED-2 and OLED-4: (k) current density–voltage (*J–V*), (l) power emitted–voltage (*P–V*).

Table 1
Electroluminescence properties of devices.

Device	Complex	L_{max}[a] (cd/m^2)	U_{on}[b] (V)	λ_{ELmax} (nm)	EQE_{max}[c] (%)	P_{emit}[d] (μWt/cm^2)
OLED-1	$Eu(dbm)_3SDZP$	360 (18 V)	3.2	613	6.7	–
OLED-2	$Yb(dbm)_3SDZP$	–	–	978	–	13.25
OLED-3	$Eu(dbm)_3SDZP$	280 (18 V)	3.4	613	3.0	–
OLED-4	$Yb(dbm)_3SDZP$	–	–	978	–	14.25

[a] L_{max}: maximum brightness.
[b] U_{on}: the turn-on voltage at 1 cd/m^2.
[c] EQE_{max}: maximum quantum efficiency.
[d] P_{emit}: power emitted.

ing or defect-related trapping, underscoring the role of the ligand in shielding the metal ion and enhancing radiative decay. Similarly, the improved PLQYs reflect a more efficient antenna effect, wherein the ligand absorbs light and transfers energy to the emitting lanthanide ion with minimal losses. These results confirm that both TDZP and SDZP act as effective antenna ligands, but the structural or electronic modifications in SDZP contribute significantly to superior photophysical properties, making it a more promising candidate for applications in lighting, sensing, or bioimaging where high luminescence efficiency and stability are required.

Based on the photoluminescence properties and the results of mobility, sufficiently intense photoluminescence of ytterbium and europium are observed for SDZP as ligand. Thus, $Eu(dbm)_3SDZP$ and $Yb(dbm)_3SDZP$ can be recommended as emission layer materials for OLED.

Based on the mobility data, the complexes with SDZP as the ligand exhibit higher electron mobility than hole mobility. To enhance the hole mobility and balance the carrier transport, a host:emitter system containing a hole-transporting host capable of efficient energy transfer to the emitter must be employed. Therefore, to achieve better luminescent performance, based on our previous works, we adopted TCTA and OXD-7 as mixed host materials (ratio of 1 emitter: 6TCTA: 3OXD-7) in emission layer (EML) and used PVK or poly-TPD as hole-transporting layers (HTL), respectively [19,33–36]. Complexes $Ln(dbm)_3SDZP$ were tested in solution-processed OLEDs named OLED-1 and OLED-2 with heterostructure ITO/PEDOT:PSS/PVK/EML/TPBi/LiF/Al, and OLEDs named OLED-3 and OLED-4 with heterostructure ITO/PEDOT:PSS/poly-TPD/EML/TPBi/LiF/Al (Figs. 5a and b). The molecular structures of these materials are presented in Fig. 5c. The EL spectra of OLEDs are presented in Figs. 5d–g. The EL characteristics of OLEDs are presented in Figs. 5h–l and Table 1.

These OLED devices exhibit characteristic luminescence from central lanthanide ions (Eu^{3+} or Yb^{3+}), and there are no ligand or host emission in the EL spectrum of all the devices, which proves that the energy is effectively confined to the Ln^{3+} ion. Notably, OLED-2 reaches a EQE_{max}% of 6.7 %, ranking among the highest reported values for Eu-based complex solution-processed OLEDs (Table S7 in Supporting information) [8,37–41].

This performance improvement primarily stems from the synergistic effect of the excited-state lifetime and charge carrier mobility. The large atomic radius of Se significantly expands the π-conjugation and molecular orbitals of the ligand, greatly enhancing intermolecular ordered π-π stacking in the solid-state films of the complexes. Consequently, the SDZP complexes exhibit a carrier mobility approximately one order of magnitude higher than TDZP, significantly improving charge injection balance within the emission layer. Their high bipolar mobility effectively facilitates balanced charge transport and spatial diffusion, broadening the exciton recombination zone and suppressing non-radiative quenching, while the slightly longer excited-state lifetime ensures efficient exciton diffusion at the recombination interface. It is precisely the synergy between the long excited-state lifetime and high electron mobility of these complexes that reduces exciton quenching caused by imbalanced carrier transport and enhances exciton utilization efficiency by extending the radiative recombination time window, thus finally enabling the devices to achieve a higher EQE_{max}%.

In summary, this study designed and synthesized four mixed-ligand complexes based on Eu^{3+} and Yb^{3+} with dbm^- as anion ligand and TDZP or SDZP as neutral ligands. SDZP-containing complexes demonstrated prolonged excited-state lifetimes and significantly higher PLQY than TDZP-based counterparts in both powder state and THF-processed films. Systematic investigation through theoretical calculations and experimental data elucidated the relationship between electronic distribution, charge mobility, and electroluminescent performance. All devices exhibited characteristic lanthanide emission. Specifically, the Eu-based OLED achieved a EQE_{max}% of 6.7 %. This integrated computational-experimental approach thereby establishes a viable strategy for developing high-efficiency lanthanide-complex OLEDs. Looking ahead, the Se-modified ligand strategy can be extended to other lanthanide complexes (*e.g.*, Tb^{3+}, Dy^{3+}) for multi-color high-efficiency OLEDs,

while the Yb-based NIR devices hold promise for advancing low-power biomedical sensors with optimized film-forming processes.

CRediT authorship contribution statement

Zhipeng Guo: Writing – original draft, Methodology, Investigation, Formal analysis, Data curation, Conceptualization. **Arseny Gladkikh:** Methodology, Formal analysis, Data curation. **Egor Latipov:** Investigation, Formal analysis. **Andrey Vashchenko:** Validation, Formal analysis. **Yaxuan Liu:** Visualization, Validation, Software. **Alexey Medvedko:** Investigation, Formal analysis, Conceptualization. **Alexander Goloveshkin:** Investigation, Formal analysis. **Olga Maloshitskaya:** Visualization, Validation. **Alexey Alexandrov:** Validation. **Aowei Zhou:** Visualization, Formal analysis. **Yiming Yin:** Visualization, Validation. **Yanan Zhu:** Writing – review & editing, Supervision, Funding acquisition, Conceptualization. **Hong Meng:** Writing – review & editing, Supervision. **Valentina Utochnikova:** Writing – review & editing, Supervision, Conceptualization.

Declaration of competing interest

The authors declare that they have no known competing financial interests or personal relationships that could have appeared to influence the work reported in this paper.

Acknowledgments

We acknowledge the financial support from the National Natural Science Foundation of China (No. 12404460), the National Key Research and Development Program of China (No. 2023YFB3608902), the Shenzhen Science and Technology Program (No. JCYJ20241202130509013), AI for Science (AI4S)-Preferred Program of Peking University, and the Guangdong Basic and Applied Basic Research Foundation (No. 2025A1515011373).

Supplementary materials

Supplementary material associated with this article can be found, in the online version, at doi:10.1016/j.cclet.2025.112136.

References

[1] C.W. Tang, S.A. VanSlyke, Appl. Phys. Lett. 51 (1987) 913–915.
[2] K. Xu, J. Zheng, F. Zhan, et al., Chem. Eng. J. 506 (2025) 159948.
[3] D.A. Shariaty, J. Schaab, E. McClure, et al., Inorg. Chem. 64 (2025) 1228–1240.
[4] C.P. Han, C.H. Hsu, C.Y. Chu, et al., Org. Electron. 138 (2025) 107178.
[5] Y. Ma, C.M. Che, H.Y. Chao, et al., Adv. Mater. 11 (1999) 852–857.
[6] X. Zhang, X. Jin, Y. Li, Chin. Chem. Lett. 33 (2022) 2117–2120.
[7] V.R. Sastri, J.R. Perumareddi, V.R. Rao, et al., Modern Aspects of Rare Earths and Their Complexes, Elsevier, 2003.
[8] V.V. Utochnikova, Lanthanide complexes as OLED emitters, in: J.C.G. Bünzli, V.K. Pecharsky (Eds.), Handbook on the Physics and Chemistry of Rare Earths, Elsevier, 2021, pp. 1–91.
[9] X. Guo, B. Li, Acta Laser Biol. Sin. 30 (2021) 193–199.
[10] X. Yang, S. Xu, Y. Zhang, et al., Angew. Chem. Int. Ed. 62 (2023) e202309739.
[11] H.L. Wang, B. Yu, F.P. Liang, H.H. Zou, Chin. Chem. Lett. 37 (2026) 111346.
[12] A.I. Kornikov, M.I. Kozlov, A.A. Vashchenko, et al., ACS Appl. Opt. Mater. 1 (2023) 1227–1235.
[13] V.V. Utochnikova, A.N. Aslandukov, A.A. Vashchenko, et al., Dalton Trans. 50 (2021) 12806–12813.
[14] A. Pereira, G. Conte, H. Gallardo, et al., J. Soc. Inf. Disp. 19 (2012) 793–797.
[15] E. Girotto, A. Pereira, C. Arantes, et al., J. Lumin. 208 (2019) 57–62.
[16] V.V. Utochnikova, A.Y. Grishko, D.S. Koshelev, et al., Opt. Mater. 74 (2017) 201–208.
[17] L. Wang, Z. Zhao, C. Wei, et al., Adv. Opt. Mater. 7 (2019) 1801256.
[18] A. Yu. Gladkikh, M.A. Sandzhieva, A. Mahmoodpoor, et al., Adv. Opt. Mater. 13 (2025) e00702.
[19] L.R. Melby, N.J. Rose, E. Abramson, J.C. Cari, J. Am. Chem. Soc. 86 (1964) 5117–5125.
[20] M.I. Kozlov, A.N. Aslandukov, A.A. Vashchenko, et al., Dalton Trans. 48 (2019) 17298–17309.
[21] M.I. Kozlov, A.A. Vashchenko, A.A. Pavlov, et al., Phys. Chem. Chem. Phys. 25 (2023) 20042–20048.
[22] M. J.Frisch, G. W.Trucks, H. B.Schlegel, et al., Gaussian 09, Revision A.03, Wallingford CT, 2009.
[23] S. Grimme, J. Antony, S. Ehrlich, H. Krieg, J. Chem. Phys. 132 (2010) 154104.
[24] J.P. Perdew, M. Ernzerhof, K. Burke, J. Chem. Phys. 105 (1996) 9982–9985.
[25] S. Grimme, S. Ehrlich, L. Goerigk, J. Comput. Chem. 32 (2011) 1456–1465.
[26] T. Lu, F. Chen, J. Comput. Chem. 33 (2012) 580–592.
[27] T. Lu, J. Chem. Phys. 161 (2024) 082503.
[28] Y. Du, H. Zhang, X. Du, et al., Appl. Sci. 15 (2025) 959.
[29] S. Bag, M. Jain, P.K. Maiti, J. Phys. Chem. B 120 (2016) 9142–9151.
[30] W.Q. Deng, L. Sun, J.D. Huang, et al., Nat. Protoc. 10 (2015) 632–642.
[31] Z. Zhao, D. Liu, J.W.Y. Lam, et al., Sci. China Chem. 53 (2010) 2311–2317.
[32] Z. Zhang, Y. Zhu, Y. Wu, C. Zhao, H. Meng, Adv. Theor. Simul. 4 (2021) 2100236.
[33] A.N. Aslandukov, V.V. Utochnikova, D.O. Goriachiy, et al., Dalton Trans. 47 (2018) 16350–16357.
[34] V.V. Utochnikova, N.N. Solodukhin, A.N. Aslandukov, et al., Org. Electron. 44 (2017) 85–93.
[35] D.S. Koshelev, A.V. Kirianova, E.Y. Korneeva, et al., Inorg. Chem. Commun. 171 (2025) 113636.
[36] M.I. Kozlov, K.M. Kuznetsov, A.S. Goloveshkin, et al., Materials 16 (2023) 959.
[37] R. Ilmi, X. Xia, J.D.L. Dutra, et al., ACS Appl. Electron. Mater. 6 (2024) 2624–2638.
[38] R. Ilmi, X. Li, N.K. Al Rasbi, et al., Dalton Trans. 52 (2023) 12885–12891.
[39] X. Li, J. Yin, J. Wang, et al., Front. Chem. 10 (2022) 965927.
[40] R. Ilmi, J. Wang, J.D.L. Dutra, et al., Chemistry 29 (2023) e202300376.
[41] M.S. Khan, R. Ilmi, W. Sun, et al., J. Mater. Chem. C 8 (2020) 5600–5612.